# An Unusual Ligand Coordination Gives Rise to a New Family of Rhodium Metalloinsertors with Improved Selectivity and Potency

Alexis C. Komor and Jacqueline K. Barton*

Division of Chemistry and Chemical Engineering, California Institute of Technology, Pasadena California 91125, United States

Ⓢ *Supporting Information*

ABSTRACT: Rhodium metalloinsertors are octahedral complexes that bind DNA mismatches with high affinity and specificity and exhibit unique cell-selective cytotoxicity, targeting mismatch repair (MMR)-deficient cells over MMR-proficient cells. Here we describe a new generation of metalloinsertors with enhanced biological potency and selectivity, in which the complexes show Rh−O coordination. In particular, it has been found that both Δ- and Λ-[Rh(chrysi)(phen)(DPE)]$^{2+}$ (where chrysi =5,6 chrysenequinone diimmine, phen =1,10-phenanthroline, and DPE = 1,1-di(pyridine-2-yl)ethan-1-ol) bind to DNA containing a single CC mismatch with similar affinities and without racemization. This is in direct contrast with previous metalloinsertors and suggests a possible different binding disposition for these complexes in the mismatch site. We ascribe this difference to the higher pK_a of the coordinated immine of the chrysi ligand in these complexes, so that the complexes must insert into the DNA helix with the inserting ligand in a buckled orientation; spectroscopic studies in the presence and absence of DNA along with the crystal structure of the complex without DNA support this assignment. Remarkably, all members of this new family of compounds have significantly increased potency in a range of cellular assays; indeed, all are more potent than cisplatin and *N*-methyl-*N*′-nitro-nitrosoguanidine (MNNG, a common DNA-alkylating chemotherapeutic agent). Moreover, the activities of the new metalloinsertors are coupled with high levels of selective cytotoxicity for MMR-deficient versus proficient colorectal cancer cells.
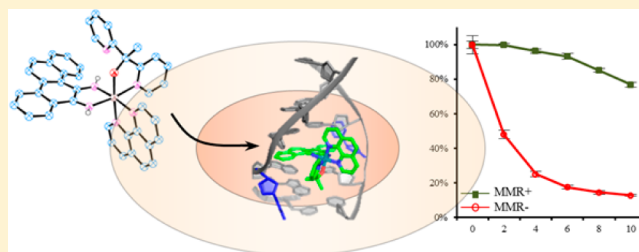
INTRODUCTION

Since the successful application of cisplatin (*cis*-diamminedichloroplatinum) as an anticancer drug, the field of inorganic medicinal chemistry has undergone a revolution.[1−4] For many years, the field focused on the development of more potent analogues (second- and third-generation derivatives), leading to the FDA approval of two additional *cis*-platinum(II) complexes, carboplatin and oxaliplatin.[5] Cisplatin and carboplatin, in particular, have been highly successful in the treatment of a variety of cancers, including testicular, ovarian, cervical, and non-small cell lung cancers.[6] However, these treatments are often associated with severe side effects and a buildup of resistance. These issues have led to a shift in the design of chemotherapeutics; researchers have begun to focus on a new design strategy where the chemotherapeutic interacts with a specific biological target found predominantly in cancer cells.[7]

The proposed mechanism of action of classical platinum-based chemotherapeutics is the formation of covalent DNA adducts, followed by cellular processing of these lesions, ultimately leading to apoptosis.[6] The synthesis of new-generation classical therapeutics with enhanced DNA-binding properties in order to increase cytotoxicity has been extensively explored. However, the design and synthesis of therapeutics which bind to specific DNA lesions that are more prevalent in cancer cells than healthy cells may represent a targeted strategy for new chemotherapy. In particular, our laboratory has focused on the development of rhodium metalloinsertors (Figure 1), which bind mismatches in duplex DNA with high specificity, preferentially targeting thermodynamically destabilized mismatches over matched base pairs by a factor of over 1000.[8,9] The binding mode of these complexes to mismatched DNA was subsequently crystallographically determined; the wide aromatic chrysi (chrysi = 5,6 chrysenequinone diimmine) ligand inserts into the DNA from the minor groove and ejects both mismatched bases in a binding mode termed metalloinsertion.[10,11] Ejection of the mismatched bases results in a large lesion that we have suggested may serve as a unique target within the cell.

Mismatches in genomic DNA arise naturally as a consequence of replication, but, if left uncorrected, can lead to mutations.[12,13] The mismatch repair (MMR) pathway serves as a checkpoint to increase the fidelity of DNA replication ~1000 fold.[14] Importantly, deficiencies in the mismatch repair machinery have been associated with several types of cancer as well as increased resistance to classical chemotherapeutics such as cisplatin as well as commonly used DNA-alkylating therapeutics.[15] Therefore, the development of a targeted therapy for MMR-deficient cancers would be invaluable in the clinic. Due to the unique DNA mismatch-binding

rac-[Rh(chrysi)(phen)(DPE)]$^{2+}$
K_B(CC): 5.4 x 10^6 M^{-1}

rac-[Rh(chrysi)(phen)(PPE)]$^{2+}$
K_B(CC): 2.6 x 10^6 M^{-1}

rac-[Rh(chrysi)(phen)(PPO)]$^{2+}$
K_B(CC): 5.5 x 10^6 M^{-1}

rac-[Rh(chrysi)(phen)(PyOctanol)]$^{2+}$
K_B(CC): 3.6 x 10^6 M^{-1}

Δ-[Rh(chrysi)(phen)(DPE)]$^{2+}$
K_B(CC): 6.0 x 10^6 M^{-1}

Λ-[Rh(chrysi)(phen)(DPE)]$^{2+}$
K_B(CC): 5.7 x 10^6 M^{-1}
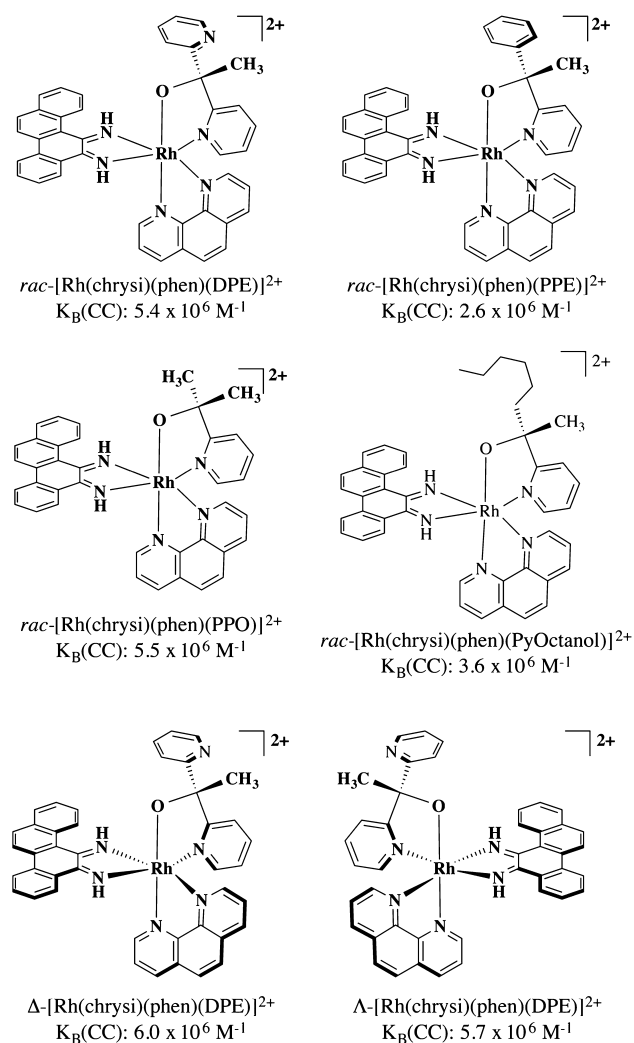
Figure 1. Chemical structures of metalloinsertors and binding affinities for oligonucleotides containing CC mismatches. All DNA binding affinities were measured in 100 mM NaCl, 20 mM NaP$_i$, pH 7.1 buffer on the duplex 36-mer with the sequence 3′-GCG ATG CAG ATA TAC **C**TA CTA GGA TTC ACT GTC ATG-5′ on one strand (underline denotes the mismatch) in a competition assay through photocleavage by [Rh(bpy)$_2$chrysi]$^{3+}$. Samples were irradiated and electrophoresed through a 20% denaturing PAGE gel, and the percent of DNA cleavage at each concentration was plotted as a function of log [Rh]. The data were fitted to a sigmoidal curve, and K_B values were determined by calculating the concentration of rhodium at the inflection points of the curve and solving simultaneous equilibria.

properties of rhodium metalloinsertors and the structural perturbation to DNA, their biological properties in MMR-deficient cells were investigated. The compounds have been found to inhibit growth and induce necrosis selectively in MMR-deficient colorectal cancer cells over MMR-proficient cells.[16,17]

Recently in our laboratory, a family of 10 metalloinsertors with varying lipophilicites yet similar mismatch binding affinities was synthesized. Their abilities to preferentially target MMR-deficient cells over MMR-proficient cells were found to vary dramatically.[18] One metalloinsertor in particular, [Rh(chrysi)(phen)(DPE)]$^{2+}$ (Figure 1, DPE = 1,1-di-(pyridine-2-yl)ethan-1-ol), was found to possess enhanced potency and selectivity compared to the others. Crystallization of the compound revealed the solid-state structure shown in

Figure 2; the DPE ligand was discovered to coordinate to the rhodium center via one pyridine ring and the alcohol oxygen, in contrast to all other previously reported metalloinsertors, which coordinate via two pyridine nitrogens (Figure S2). It was hypothesized that this new ligand coordination environment was responsible for the enhanced biological activity of this compound, and we thus sought to synthesize a family of compounds inspired by this new ligand scaffold.

In this report, we describe the discovery of an unusual ligand coordination for the rhodium metalloinsertor [Rh(chrysi)-(phen)(DPE)]$^{2+}$ and subsequent development of a family of compounds based on this new type of coordination environment. The entire family of compounds has been found to possess enhanced potency and cell selectivity in our cellular assays. In fact, all compounds studied are more potent than the FDA-approved chemotherapeutic cisplatin. All compounds have binding affinities for CC mismatches that range from 2.6 to 5.5 × 10^6 M^{-1}, comparable to previous metalloinsertors. However, the amount of intracellular rhodium required for optimal biological activity for this family of compounds is more than five times lower than that of previously reported metalloinsertors, thus making them potent in the nanomolar concentration range. Importantly, all of the complexes exhibit a highly selective cytotoxicity for cells that are deficient versus proficient in MMR.

■ EXPERIMENTAL SECTION

Materials. Commercially available chemicals were used as received. All organic reagents and Sephadex ion-exchange resin were obtained from Sigma-Aldrich unless otherwise noted. Sep-pak C$_{18}$ solid-phase extraction (SPE) cartridges were purchased from Waters Chemical Co. (Milford, MA). Media and supplements were purchased from Invitrogen (Carlsbad, CA). Bromodeoxyuridine (BrdU), antibodies, buffers, peroxidase substrate, 3-(4,5-dimethylthiazol-2-yl)-2,5-diphenyltetrazolium bromide (MTT), and acidified lysis buffer (10% SDS in 10 mM HCl) solution were purchased in kit format from Roche Molecular biochemical (Mannheim, Germany).

Oligonucleotide Synthesis and Purification. Oligonucleotides were synthesized using standard phosphoramidite chemistry at IDT DNA (Coralville, IA) and purified by HPLC using a C$_{18}$ reverse-phase column (Varian, Inc.) on a Hewlett-Packard 1100 HPLC. Quantification was performed on a Cary 100 Bio UV−vis spectrophotometer using extinction coefficients at 260 nm (ε_{260}) estimated for single-stranded DNA.

Synthesis and Characterization of Ligands and Metal Complexes. The complexes [Rh(bpy)$_2$(chrysi)]$^{3+}$ and [Rh(HDPA)$_2$-(chrysi)]$^{3+}$ were prepared according to published procedures.[19,20]

[Rh(chrysi)(phen)(NH$_3$)$_2$]Cl$_3$. According to an adaptation of previously described procedures,[21] [Rh(chrysi)(phen)(NH$_3$)$_2$]Cl$_3$ was prepared. A 1 L round-bottomed flask was charged with [Rh(NH$_3$)$_4$(phen)][OTf]$_3$ (0.500 g, 0.626 mmol), chrysene-5,6-dione (0.162 g, 0.626 mmol), and 1:9 H$_2$O:MeCN was added (400 mL). A 1 M solution of NaOH (1.5 mL) was added to the orange solution. Over the next hour, the solution changed color from orange to red, after which time a 1 M solution of HCl (1.5 mL) was added to quench the reaction. The MeCN was evaporated *in vacuo*, and the resulting red solution was loaded onto a SPE cartridge, eluted with 25% acetonitrile in 0.1% TFA$_{(aq)}$, and lyophilized to give a red solid. The chloride salt can be obtained from a Sephadex QAE anion exchange column equilibrated with 0.1 M MgCl$_2$. Yield: 0.536 g, 94%. ^{1}H NMR (300 MHz, d_6-DMSO): δ 13.59 (s, 1H); 13.43 (s, 1H); 9.56 (d, *J* = 5.3 Hz, 1 H); 9.16 (m, 2H); 8.93 (d, *J* = 8.3 Hz, 1H); 8.77 (d, *J* = 5.3 Hz, 1H); 8.35−8.57 (m, 7H); 8.23 (d, *J* = 8.3 Hz, 1H); 7.99 (m, 2H); 7.83 (m, 2H); 7.54 (t, *J* = 7.6 Hz, 1H); 4.95 (s, 3H); 4.79 (s, 3H). ESI-MS (cation): *m/z* calcd, 571.13 (M − 2H$^+$); obs., 570.9.

1-R-1-(Pyrid-2-yl) Ethanol (R = Pyridine, Phenyl, Methyl, Hexyl; DPE, PPE, PPO, PyOctanol). According to an adaptation of a

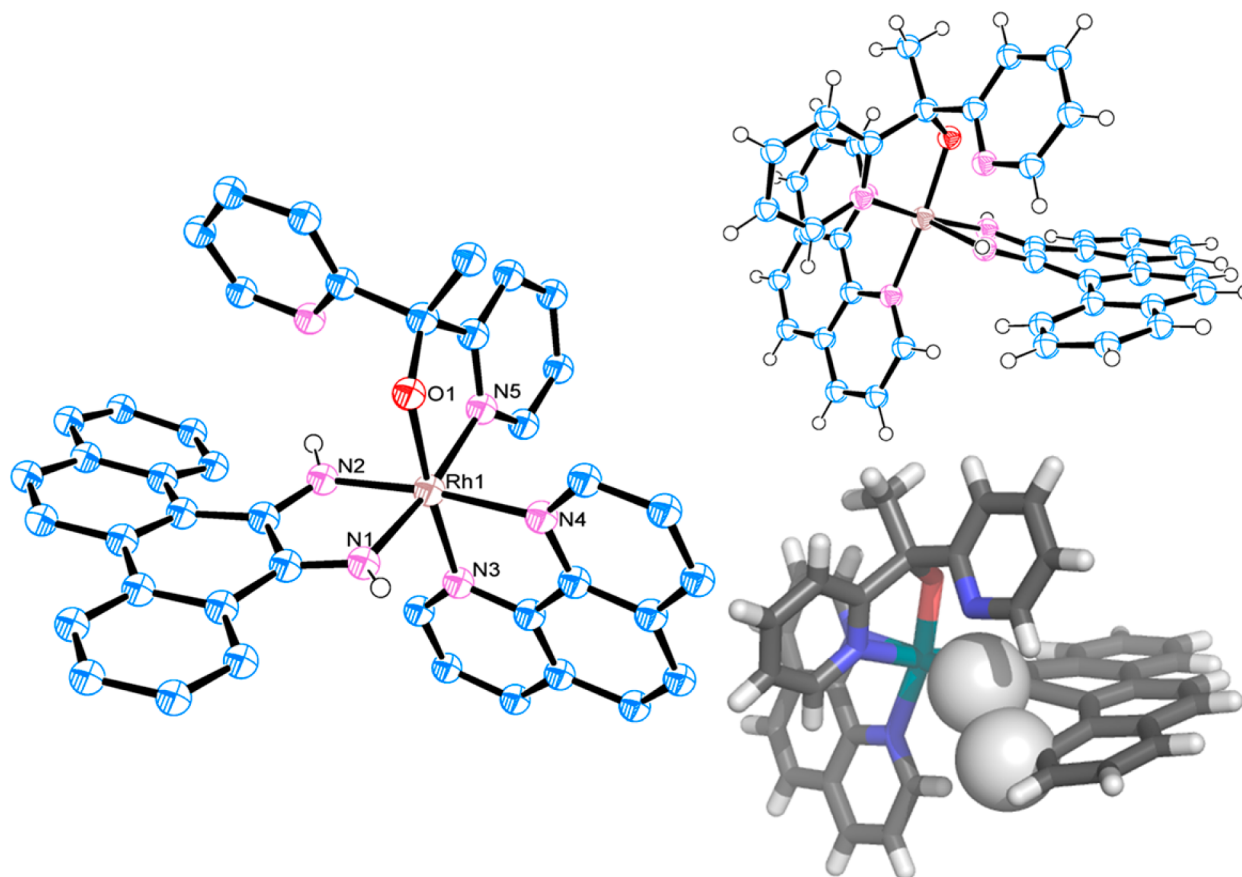**Figure 2.** Structure of a new metalloinsertor, illustrating the coordination and ligand buckling. Left: X-ray crystal structure of [Rh(chrysi)(phen)(DPE)]Cl$_2$. Displacement of ellipsoids is drawn at 50% probability. For clarity, chloride and hydrogen atoms (except immine protons) have been omitted. Top right: Side view. Note the severe distortion of the planarity of the chrysi ligand. Bottom right: View showing the steric clash responsible for the buckling of the chrysi ligand. Both hydrogens are shown as van der Waals surfaces.

previously described procedure,[22] 1-R-1-(pyrid-2-yl) ethanol (R = pyridine, phenyl, methyl, hexyl; DPE, PPE, PPO, PyOctanol) were synthesized. The appropriate ketone py(CO)(L) (8.3 mmol) was dissolved in dry diethyl ether (100 mL) in an oven-dried 250 mL Schlenk flask under Ar. The solution was cooled to −78 °C, and MeLi (12.9 mL of a 1.6 M solution) was added slowly over 15 min. The resulting yellow solution was allowed to stir at −78 °C for 1 h and then warmed to ambient temperature. Next, saturated NH$_4$Cl (aq) (30 mL) was added to quench the reaction, and the resulting solution was extracted with EtOAc (3 × 75 mL) and dried over Na$_2$SO$_4$, and the solvent evaporated *in vacuo*. The crude product was purified via flash chromatography (SiO$_2$, 1:1 EtOAc:CH$_2$Cl$_2$ for L = Me and hexyl, 1:3 EtOAc:CH$_2$Cl$_2$ for L = Ph) to afford a light-yellow oil.

1,1-Di(pyridine-2-yl)ethan-1-ol (DPE). Yield: 100%. ^{1}H NMR (CDCl$_3$, 300 MHz): δ 8.57 (d, *J* = 5.1 Hz, 2H); 7.92 (d, *J* = 6.9 Hz, 2H); 7.80 (m, 2H); 7.27 (m, 2H); 6.60 (s, 1H); 2.08 (s, 3H). ESI-MS (cation): *m/z* calcd, 201.09 (M + H^{+}); obs., 201.0.

1-Phenyl-1-(pyridine-2-yl)ethan-1-ol (PPE). Yield: 97%. ^{1}H NMR (CDCl$_3$, 300 MHz): δ 8.52 (d of m, *J* = 5.1 Hz, 1 H); 7.65 (t of d, *J* = 7.8 Hz, 1.8 Hz, 1 H); 7.48 (m, 2H); 7.31 (m, 3H); 7.17−7.26 (m, 2H); 5.85 (s, 1H); 1.94 (s, 3H).

2-(Pyridine-2-yl)propan-2-ol (PPO). Yield: 55% ^{1}H NMR NMR (CDCl$_3$, 300 MHz): δ 8.52 (d of m, *J* = 4.8 Hz, 1 H); 7.71 (t of m, *J* = 7.8 Hz, 1 H); 7.38 (d of m, *J* = 8.1 Hz, 1H); 7.21 (t of m, *J* = 6.2 Hz, 1H); 5.08 (s, 1H); 1.54 (s, 6H).

2-(Pyridine-2-yl)octan-2-ol (PyOctanol). Yield: 35% ^{1}H NMR NMR (CDCl$_3$, 300 MHz): δ 8.51 (d of m, *J* = 6.0 Hz, 1 H); 7.71 (t of m, *J* = 9.0 Hz, 1 H); 7.32 (d of m, *J* = 9.0 Hz, 1H); 7.20 (t of m, *J* = 6.0 Hz, 1H); 5.18 (s, 1H); 1.78 (m, 2H); 1.51 (s, 3H); 1.19 (m, 6H); 0.82 (m, 5H).

[Rh(chrysi)(phen)(L)]Cl$_2$ (L = DPE, PPE, PPO, PyOctanol). According to an adaptation of a previously described method,[18] [Rh(chrysi)(phen)(L)]Cl$_2$ (L = DPE, PPE, PPO, PyOctanol) were prepared. [Rh(chrysi)(phen)(NH$_3$)$_2$]TFA$_3$ (62.3 mg, 0.092 mmol) and L (0.138 mmol) were dissolved in 1:12 H$_2$O:EtOH (90 mL). The resulting red solution was heated to 98 °C and allowed to reflux for 18 h. The resulting solution was dried *in vacuo*, redissolved in H$_2$O (10 mL), filtered, and purified via flash chromatography (C$_{18}$−SiO$_2$, 17:3 0.1% TFA (aq): MeCN). All compounds but [Rh(chrysi)(phen)-(PyOctanol)]$^{2+}$ were synthesized as a mixture of diastereomers; only the diasteriomers of [Rh(chrysi)(phen)(DPE)]$^{2+}$ were resolvable via HPLC (17:3 0.1% TFA (aq): MeCN to 1:1 0.1% TFA (aq): MeCN gradient over 45 min). The chloride salt can be obtained from a Sephadex QAE anion exchange column equilibrated with 0.1 M MgCl$_2$.

[Rh(chrysi)(phen)(DPE)]Cl$_2$. Yield: 30%. ESI-MS (cation): *m/z* calcd, 737.15 (M − H^{+}), 369.1 (M^{2+}); obs., 737, 369. UV−vis (H$_2$O, pH 7): 272 nm (102,100 M^{-1} cm^{-1}), 303 nm (35,400 M^{-1}, cm^{-1}), 440 nm (10,600 M^{-1}, cm^{-1}). ^{1}H NMR (CD$_3$CN, 500 MHz): δ 15.10 (s, 1 H); 11.30 (s, 1 H); 9.62 (d, *J* = 5.5 Hz, 1H); 8.98 (d, *J* = 7.0 Hz, 1H); 8.92 (d, *J* = 8.0 Hz, 1H); 8.88 (m, 2H); 8.36 (m, 4H); 8.27 (d, *J* = 8.5 Hz, 1H); 8.21 (m, 1H); 8.13 (d, *J* = 8.5 Hz, 1H); 8.00 (m, 2H); 7.94 (d, *J* = 8.5 Hz, 1H); 7.73−7.78 (m, 4H); 7.62 (t, *J* = 8.0 Hz, 1H); 7.57 (d, *J* = 8.0 Hz, 1H); 7.50 (t, *J* = 7.0 Hz, 1H); 7.32 (d, *J* = 6.5 Hz, 1H); 7.14 (m, 1H); 6.95 (t, *J* = 7.5 Hz, 1H); 6.33 (t, *J* = 6.0 Hz, 1H); 1.98 (s, 3H). Crystals suitable for X-ray diffraction were obtained from vapor diffusion of diethyl ether into a concentrated solution of [Rh(chrysi)(phen)(DPE)]Cl$_2$ dissolved in ethanol.

[Rh(chrysi)(phen)(PPE)]Cl$_2$. Yield: 80%. ESI-MS (cation): *m/z* calcd, 736.2 (M − 1H[+]), 368.6 (M^{2+}); obs., 736.0, 368.8. UV−vis (H$_2$O, pH 7): 270 nm (165,800 M^{-1} cm^{-1}), 300 nm (56,300 M^{-1}

cm^{-1}), 430 nm (16,100 M^{-1} cm^{-1}). ^{1}H NMR (CD$_3$CN, 600 MHz): δ 15.45 (s, 1 H); 14.38 (s, 1 H); 11.76 (s, 1 H); 11.08 (s, 1 H); 9.71 (d, J = 5.2 Hz, 1H); 9.49 (d, J = 5.2 Hz, 1H); 9.12 (d, J = 5.6 Hz, 1H); 8.99 (d, J = 9.0 Hz, 1H); 8.94 (m, 2H); 8.88 (m, 3H); 8.81 (d, J = 8.0 Hz, 1H); 8.46 (d, J = 8.0 Hz, 1H); 8.35–8.39 (m, 4H); 8.29–8.33 (m, 3H); 8.20–8.25 (m, 4H); 8.14 (t, J = 8.0 Hz, 1H); 8.10 (m, 2H); 8.03 (m, 1H); 7.99 (m, 1H); 7.92 (d, J = 7.5 Hz, 1H); 7.89 (d, J = 8.5 Hz, 1H); 7.83 (m, 1H); 7.68–7.80 (m, 5H); 7.64 (m, 1H); 7.55–7.60 (m, 4H); 7.52 (m, 2H); 7.40 (d, J = 5.7 Hz, 1H); 7.28–7.34 (m, 4H); 7.23 (t, J = 6.6 Hz, 1H); 7.16 (m, 3H); 6.61 (t, J = 6.6 Hz, 2H); 6.33 (t, J = 6.6 Hz, 1H); 2.49 (s, 3H); 2.13 (s, 3H) (1:1 mixture of diasteriomers). Crystals suitable for X-ray diffraction were obtained from vapor diffusion of diethyl ether into a concentrated solution of [Rh(chrysi)-(phen)(PPE)]Cl$_2$ dissolved in methanol.

[Rh(chrysi)(phen)(PPO)]Cl$_2$. Yield: 40%. ESI-MS (cation): *m/z* calcd, 674.1 (M − 1H$^+$), 337.6 (M^{2+}); obs., 674.0, 337.7. UV−vis (H$_2$O, pH 7): 270 nm (122,400 M^{-1} cm^{-1}), 300 nm (41,600 M^{-1} cm^{-1}), 430 nm (12,300 M^{-1} cm^{-1}). ^{1}H NMR (CD$_3$CN, 500 MHz): δ 13.29 (br s, 1.7 H); 11.68 (br s, 1 H); 9.61 (d, J = 5.2 Hz, 1H); 9.54 (d, J = 5.2 Hz, 1.7H); 9.09 (d, J = 5.5 Hz, 1H); 8.93 (m, 5.4H); 8.88 (m, 2.7H); 8.30–8.42 (m, 12.5H); 8.26 (m, 1H); 8.23 (m, 1.7H); 8.14 (m, 4.4H); 7.93–8.04 (m, 11.5H); 7.74–7.85 (m, 5.4H); 7.55 (m, 4.4H); 7.49 (t, J = 8.0 Hz, 1H); 7.21 (m, 2H); 7.13 (m, 1H); 7.09 (m, 2.7H); 2.00 (s, 3H); 1.96 (s, 5.1H); 1.67 (s, 3H); 1.66 (s, 5.1H); (1:1.7 mixture of diasteriomers). Crystals suitable for X-ray diffraction were obtained from vapor diffusion of diethyl ether into a concentrated solution of [Rh(chrysi)(phen)(PPO)]Cl$_2$ dissolved in isopropanol.

[Rh(chrysi)(phen)(PyOctanol)]Cl$_2$. Yield: 10%. ESI-MS (cation): *m/z* calcd 744.2 (M − 1H$^+$), 372.6 (M^{2+}); obs., 744.1, 372.8). ^{1}H NMR (CD$_3$CN, 500 MHz): δ 15.00 (s, 1 H); 12.80 (s, 1 H); 9.55 (d, J = 5.0 Hz, 1H); 9.12 (d, J = 8.0 Hz, 1H); 9.09 (d, J = 5.5 Hz, 1H); 8.94 (d, J = 8.9 Hz, 1H); 8.88 (d, J = 8.5 Hz, 1H); 8.85 (d, J = 8.5 Hz, 1H); 8.32–8.44 (m, 5H); 8.17 (m, 2H); 8.08 (m, 1H); 7.91 (t, J = 7.0 Hz, 1H); 7.86 (t, J = 8.0 Hz, 1H); 7.80 (m, 2H); 7.54 (t, J = 7.5 Hz, 1H); 7.41 (d, J = 8.0 Hz, 1H); 7.31 (d, J = 6.0 Hz, 1H); 7.05 (t, J = 7.0 Hz, 1H); 1.74 (s, 3H); 1.55 (m, 2H); 0.71–0.96 (m, 11H).

Crystals of [Rh(HDPA)$_2$(chrysi)]Cl$_2$ (one chrysi immine deprotonated) suitable for X-ray diffraction were obtained from vapor diffusion of diethyl ether into a concentrated solution of [Rh(HDPA)$_2$(chrysi)]Cl$_2$ dissolved in ethanol.

Enantiomeric Separation. A 2 mM solution (1.5 mL) of [Rh(chrysi)(phen)(DPE)]$^{2+}$ was injected, 30 μL at a time, onto an Astec CYCLOBOND I 2000 Chiral HPLC Column that was heated to 40 °C. An isocratic method of 50% acetonitrile, 50% 100 mM KPF$_6$ was used to separate the two enantiomers. An automatic fraction collector was used to collect each peak separately. The resulting dilute solutions were loaded onto a SPE cartridge and rinsed with copious amounts of 0.1% TFA$_{(aq)}$. The SPE cartridge was eluted with 10% acetonitrile in 0.1% TFA$_{(aq)}$. The chloride salts were obtained from a Sephadex QAE anion exchange column equilibrated with 0.1 M MgCl$_2$. Circular dichroism spectra were taken on an Aviv 62DS spectropolarimeter in a 1 mm path length cell.

X-ray Structure Determination. Details of the structure determinations and refinements for all structures are provided in Supporting Information.

Metalloinsertor pH Titrations. Solutions (25 μM) of [Rh(chrysi)(phen)(DPE)]$^{2+}$, [Rh(chrysi)(phen)(PPE)]$^{2+}$, [Rh(chrysi)(phen)(PPO)]$^{2+}$, [Rh(bpy)$_2$(chrysi)]$^{3+}$, or [Rh(HDPA)$_2$(chrysi)]$^{3+}$ (3 mL, in 0.1 M NaCl) were prepared, and absorption spectra measured on a Cary 100 Bio UV−vis spectrophotometer. The pH of the solutions and their blanks were adjusted (and monitored by an internal electrode) from approximately 4.5 to 10.5 and back via titration with either 6 mM NaOH or 10 mM HCl. After each acid or base addition, an absorption spectrum was taken. A single wavelength was selected for each metal complex where a large change was observed over the course of the titration. The absorbance at this wavelength was then plotted as a function of pH to generate a titration curve. The pK_a of each metal complex was determined from the inflection point of this sigmoidal curve. The data

from three separate experiments were pooled to determine average pK_a values.

In addition, 25 μM solutions of 1:1 [Rh(chrysi)(phen)-(DPE)]$^{2+}$:DNA, [Rh(chrysi)(phen)(PPE)]$^{2+}$:DNA, [Rh(chrysi)-(phen)(PPO)]$^{2+}$:DNA, or [Rh(HDPA)$_2$(chrysi)]$^{3+}$:DNA (3 mL, in 100 mM NaCl, 20 mM NaP$_i$, pH 7.1 buffer) were prepared and absorption-spectra measured on a Cary 100 Bio UV−vis spectrophotometer. The DNA hairpin 5′-GGCAGG<u>C</u>ATGGCTTTTTGC-CATC<u>C</u>CTGCC-3′ (underline denotes the CC mismatch) was used.

Photocleavage Competition Titrations. The oligonucleotide 3′-GCG ATG CAG ATA TAC <u>C</u>TA CTA GGA TTC ACT GTC ATG-5′ was ^{32}P-labeled at the 5′-end by incubating DNA with ^{32}P-ATP and polynucleotide kinase (PNK) at 37 °C for 2 h, followed by purification using gel electrophoresis. A small amount of the labeled DNA (<1% of the total amount of DNA) was added to 2 μM unlabeled DNA and its corresponding unlabeled complement (with a CC mismatch incorporated at the underlined site) in 100 mM NaCl, 20 mM NaP$_i$, pH 7.1 buffer. The duplex DNA was annealed by heating at 90 °C for 10 min and cooling slowly to ambient temperature over a period of 2 h. Solutions of non-photocleaving rhodium complex ranging from nanomolar to micromolar concentration as well as a 4 μM [Rh(bpy)$_2$(chrysi)]$^{3+}$ solution were made in Milli-Q water. Annealed 2 μM DNA (10 μL), 4 μM [Rh(bpy)$_2$(chrysi)]$^{3+}$ (5 μL), and 5 μL of non-photocleaving Rh solution at each concentration were mixed in a microcentrifuge tube and incubated at 37 °C for 10 min. A light control ($\emptyset$Rh), in which the DNA was mixed with 10 μL of water and irradiated, and a dark control ($\emptyset$hν), in which the DNA was mixed with the highest concentration of rhodium complex without irradiation, were also prepared. The samples were then irradiated on an Oriel (Darmstadt, Germany) 1000 W Hg/Xe solar simulator (340−440 nm) for 15 min. The samples were dried and electrophoresed in a 20% denaturing polyacrylamide gel. The gel was then exposed to a phosphor screen, and the relative amounts of DNA in each band were quantitated by phosphorimagery (ImageQuant).

Multiple Sequence Contexts. The oligonucleotide hairpins of the sequences 5′-GGCAGT<u>X</u>CTGGCTTTTTGCCAG<u>Y</u>ACTGCC-3′ (<u>XY</u> = CC, CA, CT, AA) were ^{32}P-labeled at the 5′-end as described above. Samples of labeled DNA were combined with unlabeled carrier and annealed as described. Solutions of Δ- and Λ-[Rh(chrysi)(phen)-(DPE)]$^{2+}$ ranging from 0.5 μM to 2 mM as well as either 4 μM (CC and CT mismatches) or 20 μM (CA and AA mismatches) [Rh(bpy)$_2$(chrysi)]$^{3+}$ solutions were made in Milli-Q water. Annealed 2 μM DNA (10 μL), 4 or 20 μM [Rh(bpy)$_2$(chrysi)]$^{3+}$ (5 μL), and 5 μL of Δ- or Λ-[Rh(chrysi)(phen)(DPE)]$^{2+}$ solution at each concentration was mixed in a microcentrifuge tube and incubated at 37 °C for 10 min. Samples were then irradiated and electrophoresed as described above.

Binding Constant Determination. The fraction of DNA cleaved in each lane on the gel (see Figure S5 for a typical autoradiogram) was normalized and plotted against the log of the concentration of rhodium complex. The data were fit to a sigmoidal curve using OriginPro 6.1 (Figure S6). The resulting midpoint value (i.e., the log of [rhodium complex] at the inflection point of the curve) was converted to units of concentration ([Rh$_{50\%}$]). The binding and dissociation constants of the non-photocleaving complex were determined by solving simultaneous equilibria involving DNA, [Rh(bpy)$_2$(chrysi)]$^{3+}$, and the complex in question in Mathematica 6.0. The data from at least three photocleavage titrations were averaged for each metal complex to give an average binding affinity.

Covalent DNA Binding Assay. A 6.0 μM solution (250 μL) of the DNA hairpin 5′-GGCAGG<u>C</u>ATGGCTTTTTGC-CATC<u>C</u>CTGCC-3′ (underline denotes the CC mismatch) in either in 100 mM NaCl, 20 mM NaP$_i$, pH 7.1 or 100 mM NaCl, 20 mM NaP$_i$, 5 mM glutathione (to mimic the reducing environment of the cell) was added to a 6.0 μM solution of [Rh(bpy)$_2$(chrysi)]$^{3+}$, [Rh(HDPA)$_2$(chrysi)]$^{3+}$, [Rh(chrysi)(phen)(PPE)]$^{2+}$, or H$_2$O (250 μL). The resulting solution was allowed to incubate at 37 °C for 30 min, followed by a 10 min incubation at 90 °C. A 3.0 M solution of NaOAc (50 μL) was added, followed by EtOH (1.5 mL) in order to precipitate the DNA. The resulting solution was vortexed and

incubated on dry ice for 1.5 h, after which time it was spun at 14,000 rpm for 12 min. The supernatant was discarded, and the pellet dissolved in water (100 μL) and EtOH precipitated out again. The supernatant was discarded, and the pellet dissolved in water (500 μL). An electronic absorption (UV−vis) spectrum was then taken of the resulting solution on a Cary 100 Bio UV−vis spectrophotometer.

Circular Dichroism Study of Δ/Λ-[Rh(chrysi)(phen)(DPE)]²⁺ Bound to Mismatched DNA. 50 μM solutions of the DNA hairpin 5′-GGCAGG<u>C</u>ATGGCTTTTTGCCAT<u>C</u>CCTGCC-3′ (underline denotes the CC mismatch) and Δ- and Λ-[Rh(chrysi)(phen)-(DPE)]²⁺ (200 μL in 100 mM NaCl, 20 mM NaP$_i$, pH 7.1 buffer) were prepared, and CD spectra were taken on an Aviv 62DS spectropolarimeter in a 1 mm path length cell. Each metal complex solution (100 μL) was then added to 100 μL of the DNA solution, and CD spectra were immediately recorded. After 30 min, additional CD spectra were recorded to confirm that no changes in the spectra occurred.

Cell Culture. HCT116N and HCT116O cells were grown in RPMI medium 1640 supplemented with 10% FBS; 2 mM L-glutamine; 0.1 mM non-essential amino acids; 1 mM sodium pyruvate; 100 units/mL penicillin; 100 μg/mL streptomycin; and 400 μg/mL Geneticin (G418). Cells were grown in tissue culture flasks (Corning Costar, Acton, MA) at 37 °C under 5% CO$_2$ and humidified atmosphere.

Cellular Proliferation ELISA. HCT116N and HCT116O cells were plated in 96-well plates at 2000 cells/well and allowed 24 h to adhere. The cells were then incubated with either rhodium or the appropriate chemotherapeutic (cisplatin or MNNG) for the concentration and durations specified. After 24 h, the chemotherapeutic-containing media was replaced with fresh media, and the cells were grown for the remainder of the 72 h period. Cells were labeled with BrdU 24 h before analysis. The BrdU incorporation was quantified by antibody assay according to established procedures.[23] Cellular proliferation was expressed as the ratio of the amount of BrdU incorporated by the treated cells to that of the untreated cells.

MTT Cytotoxicity Assay. Cytotoxicity assays were performed as described in the literature.[24] HCT116N and HCT116O cells were plated in 96-well plates at 50,000 cells/well and incubated with rhodium for the durations specified. After rhodium incubation, cells were labeled with MTT for 4 h at 37 °C under 5% CO$_2$ and humidified atmosphere. The resulting formazan crystals were dissolved with solubilizing reagent purchased from Roche according to the manufacturer's instructions. The dissolved formazan was quantified as the absorbance at 570 nm minus the background absorbance at 690 nm. Percent viability was determined as the ratio of the amount of formazan in the treated cells to that of the untreated cells.

Cell Death Mode Flow Cytometry Assay. Cell death was characterized by a dye exclusion assay.[25] After 24, 48-, or 72 h incubation with rhodium, cells were harvested from adherent culture by trypsinization, washed with cold PBS, and centrifuged at 2,000 rpm for 5 min. The resultant pellets were resuspended in PBS to a concentration of 10⁶ cells/mL and stained with propidium iodide to a final concentration of 1 μg/mL and YO-PRO-1 to a final concentration of 50 nM for 30 min prior to analysis by flow cytometry.

Assay for Whole-Cell Rhodium Levels. HCT116O cells were plated at 1×10^6 cells/well in a 6-well plate. The cells were allowed 24 h to adhere, then treated with 10 μM [Rh(HDPA)$_2$(chrysi)]Cl$_3$, 5 μM [Rh(chrysi)(phen)(DPE)]Cl$_2$, 1 μM [Rh(chrysi)(phen)(PPE)]Cl$_2$, or 0.5 μM [Rh(chrysi)(phen)(PPO)]Cl$_2$. After 24 h, the media was decanted, the cell monolayer washed with 3 mL PBS, and the cells lysed with 800 μL of 1% SDS. The cell lysate was sonicated on a Qsonica Ultrasonic processor for 10 s at 20% amplitude. 750 μL of the lysate was then combined with 750 μL of a 2% HNO$_3$ (v/v) solution, while the remainder of the lysate was quantified for protein by a bicinchoninic assay (BCA).[26] The 1% HNO$_3$ solution was analyzed for rhodium content on a Thermo X Series II ICP-MS unit. Rhodium counts were normalized to the amount of protein determined from the BCA analysis (to obtain ng [Rhodium]/mg [protein] values). Standard errors for three independent experiments are shown. The experiment was repeated with HCT116N cells to verify similar uptake of rhodium by the two cell lines.

■ RESULTS

Synthesis and Characterization of Compounds. Single crystals of [Rh(chrysi)(phen)(DPE)]Cl$_2$ were grown from a vapor diffusion of diethyl ether into a concentrated solution of the complex in ethanol. The solved structure revealed the DPE ligand to coordinate via the oxygen instead of the second pyridine nitrogen. In order to assess the generality of this coordination environment and to determine if the solid-state structure of [Rh(chrysi)(phen)(DPE)]Cl$_2$ is the same as its solution structure, we synthesized a phenyl (PPE) derivative and a methyl (PPO) derivative (Figure 1). Both ligands are notable in their lack of a second nitrogen to coordinate to the rhodium center. These new compounds can be synthesized via analogous methods and in reasonable yields. Single crystals grown of both compounds confirmed the generality of this unusual ligand coordination (Figures S3 and S4).

These compounds were also designed to ascertain the importance of both the ligand coordination environment (the presence of a Rh−O bond) and the bulky "dangling" pyridine group with regards to the enhanced potency and cell-selective activity of the parent compound. An additional compound with a greasy hexyl group appended to this ligand scaffold was also synthesized to assess the effects of lipophilicity on the biological activity of this family of compounds.

The acidity constants of the immine protons in [Rh(chrysi)-(phen)(DPE)]²⁺, [Rh(chrysi)(phen)(PPE)]²⁺, and [Rh(chrysi)(phen)(PPO)]²⁺ as compared to [Rh(HDPA)$_2$-(chrysi)]³⁺ and [Rh(bpy)$_2$(chrysi)]³⁺ were determined by pH spectroscopic titrations. It has previously been demonstrated that the visible absorbance changes which occur as the pH of a rhodium complex solution is titrated can be used for the determination of the pK_a values of the compounds.[27] As the pH of the solution increases from 4.5 to 11, the band centered near 440 nm (which corresponds to a charge-transfer transition between the Rh center and the chrysi ligand) undergoes a blue shift (Figures 3 and S7−S10). When the absorbance values at the initial maximum are plotted as a function of pH, a titration curve can be constructed, and the pK_a value of each metal complex can be determined from the inflection point of the curve (Figures S7−10, insets). The pK_a values for these complexes are given in Table 1. These values reflect differences in equilibrium constants of almost 2 orders of magnitude, likely due to the negative charge of the alkoxide ligands as compared to HDPA and bpy.

All three crystallographically characterized compounds are synthesized as a mixture of two diastereomers (see Experimental Section), but only the diastereomers of [Rh(chrysi)-(phen)(DPE)]²⁺ were resolvable via HPLC. The enantiomers

Table 1. pK_a Values for All Compounds As Determined by Spectrophotometric Titration[a]

compound[b]	pK_a
[Rh(bpy)$_2$(chrysi)]³⁺/²⁺	5.6 ± 0.2
[Rh(HDPA)$_2$(chrysi)]³⁺/²⁺	7.0 ± 0.5
[Rh(chrysi)(phen)(DPE)]²⁺/¹⁺	8.7 ± 0.2
[Rh(chrysi)(phen)(PPE)]²⁺/¹⁺	8.9 ± 0.4
[Rh(chrysi)(phen)(PPO)]²⁺/¹⁺	8.3 ± 0.3

[a]Titrations were performed at ambient temperature in 0.1 M NaCl solutions. Reported errors were found from repeated trials. [Rh(bpy)$_2$(chrysi)]³⁺ pK_a matches with the previously reported value of 5.2 ± 0.2.[27] [b]All compounds were used as racemic mixtures.
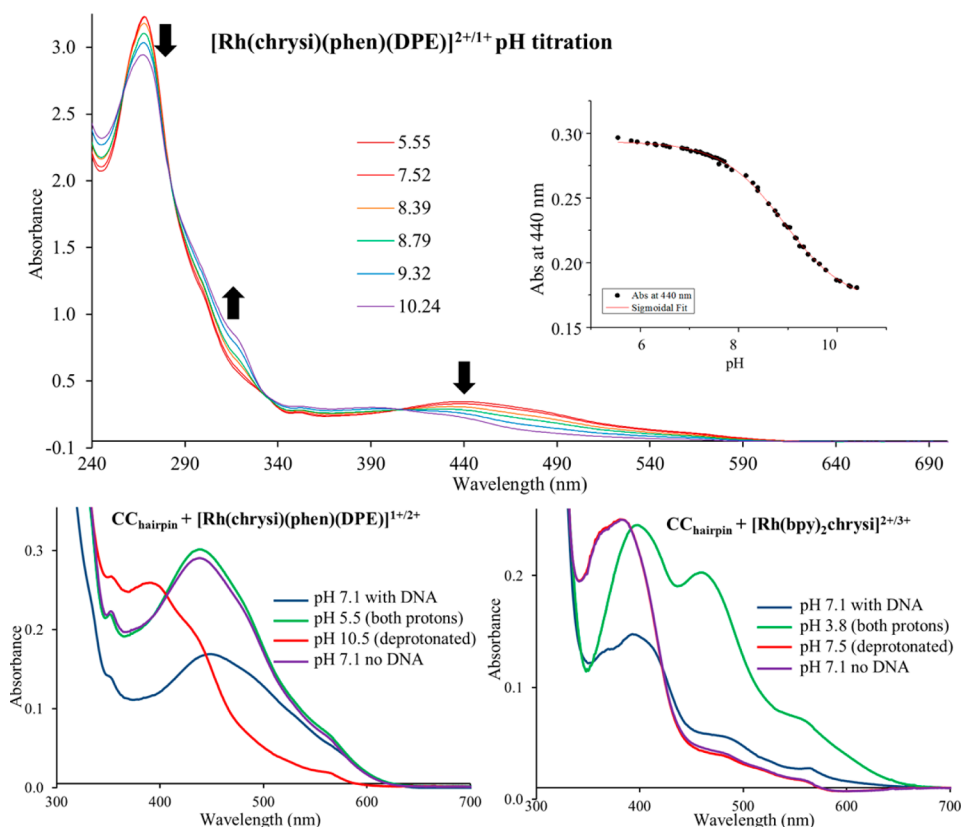
Figure 3. Top: pH titration of $[Rh(chrysi)(phen)(DPE)]^{2+}$. Shown are absorption spectra of a 25 μM solution of $[Rh(chrysi)(phen)(DPE)]^{2+}$ as the pH changes from 5.6 (red) to 10.2 (purple). The black arrows exhibit the direction in which the various bands change as the pH increases. (Inset) The absorbance at 440 nm was plotted as a function of pH and fit to a sigmoidal curve. The pK_a was determined from the inflection point of this curve. Bottom: Absorption spectra of $[Rh(chrysi)(phen)(DPE)]^{2+}$ (left) and $[Rh(bpy)_2(chrysi)]^{3+}$ (right) bound to mismatched DNA. Shown in blue are absorption spectra of 25 μM solutions of $[Rh(chrysi)(phen)(DPE)]^{2+}$ and $[Rh(bpy)_2(chrysi)]^{3+}$ with 25 μM of the DNA hairpin 5′-GGCAGG$\underline{C}$ATGGCTTTTTGCCAT$\underline{C}$CCTGCC-3′ (underline denotes the CC mismatch) in 100 mM NaCl, 20 mM NaP$_i$, pH 7.1 buffer. The absorption spectra of the species retaining the immine protons are shown in green, those of the deprotonated species are in red, and those of the compounds in 100 mM NaCl, 20 mM NaP$_i$, pH 7.1 buffer with no DNA are shown in purple.

of $[Rh(chrysi)(phen)(DPE)]^{2+}$ were separated and characterized via CD spectroscopy (Figure S11). HPLC analysis of the purified fractions confirmed >95% ee of the Δ isomer and ~90% ee of the Λ isomer (data not shown). These enantiomers are stable in aqueous solution for up to 1 month; no interconversion of the enantiomers is observed in either neutral buffer or buffer with 5 mM glutathione.

Binding of Complexes to Oligonucleotides Containing Single Base Mismatches. To ascertain the protonation states of the chrysi ligands of $[Rh(chrysi)(phen)(DPE)]^{2+}$, $[Rh(chrysi)(phen)(PPE)]^{2+}$, $[Rh(chrysi)(phen)(PPO)]^{2+}$, $[Rh(HDPA)_2(chrysi)]^{3+}$, and $[Rh(bpy)_2(chrysi)]^{3+}$ upon mismatched DNA binding, mismatched DNA was added to all compounds in a 1:1 ratio and absorption spectra recorded. As can be seen in Figure 3, $[Rh(chrysi)(phen)(DPE)]^{2+}$ binds to mismatched DNA with retention of both immine protons. Due to the extent of hypochromicity and red-shifting of the charge-transfer band, it is clear that the complex binds strongly to the mismatched DNA. In contrast, the chrysi ligand of $[Rh(bpy)_2(chrysi)]^{3+}$ is deprotonated upon mismatched DNA binding. Again, hypochromicity and red-shifting of the CT band show a strong binding of the complex to mismatched DNA. This result is consistent with the various crystal structures of $[Rh(bpy)_2(chrysi)]^{3+}$ bound to different DNA mismatches.[10,11] The other Rh−O containing compounds $[Rh(chrysi)(phen)-(PPE)]^{2+}$ and $[Rh(chrysi)(phen)(PPO)]^{2+}$ were also found to

retain both immine protons upon DNA binding (Figure S12), while $[Rh(HDPA)_2(chrysi)]^{3+}$ appears to be a mixture of protonated and deprotonated species when bound to mismatched DNA (Figure S12).

The new family of complexes does not promote DNA cleavage upon irradiation, and, as such, their binding affinities were determined through binding competition titrations with 1 μM rac-$[Rh(bpy)_2(chrysi)]^{3+}$, which does cleave DNA upon irradiation.[8,9,28] Titrations were performed with a 36-mer DNA duplex containing a CC mismatch (underlined): 3′-GCG ATG CAG ATA TAC $\underline{C}$TA CTA GGA TTC ACT GTC ATG-5′. A representative photocleavage titration can be found in Figure S5. The degree of photocleavage can be plotted against the log([Rh]) and fit to a sigmoidal curve (Figure S6). On the basis of the binding constant of $[Rh(bpy)_2(chrysi)]^{3+}$, the binding constants of all subsequent complexes are then determined by solving simultaneous equilibria at the inflection point of the photocleavage titration curve. The results are shown in Figure 1. All racemic mixtures of compounds exhibit similar binding affinities, varying from 2.6 to 5.5 × 10^6 M^{-1}. Most interesting, however, is the observation that the two enantiomers of $[Rh(chrysi)(phen)(DPE)]^{2+}$ bind to mismatched DNA with the same affinity (6.0 × 10^6 and 5.7 × 10^6 M^{-1} for Δ and Λ, respectively). This is in direct contrast to $[Rh(bpy)_2(chrysi)]^{3+}$, in which only the Δ isomer binds to mismatched DNA.[8]

Table 2. Thermodynamic Binding Constants of Δ- and Λ-[Rh(chrysi)(phen)(DPE)]²⁺ and Δ-[Rh(bpy)₂(chrysi)]³⁺ at Varied Mismatched Sites

mismatch[a]	Δ (× 10⁶ M⁻¹)	Λ (× 10⁶ M⁻¹)	[Rh(bpy)₂(chrysi)]³⁺ (× 10⁶ M⁻¹)[b]	destabilization (kcal/mol)[c]
CC	1.1	1.1	2.4	2.15
CT	0.55	1.0	4.6	2.0
CA	0.47	2.4	2.0	1.4
AA	0.23	3.5	1.6	0.8

[a]DNA binding affinities were measured in 100 mM NaCl, 20 mM NaP$_i$, pH 7.1 buffer on the 29-mer hairpins 5′-GGCAGT$\underline{X}$CTGGCTTTTTGC-CAG$\underline{Y}$ACTGCC-3′ ($\underline{XY}$ = CC, CT, CA, or AA, underline denotes the mismatch) in a competition assay through photocleavage by [Rh(bpy)₂chrysi]³⁺. [b]Binding constants all have standard errors within 10%. [c]Mismatch thermodynamic values found from ref 29.
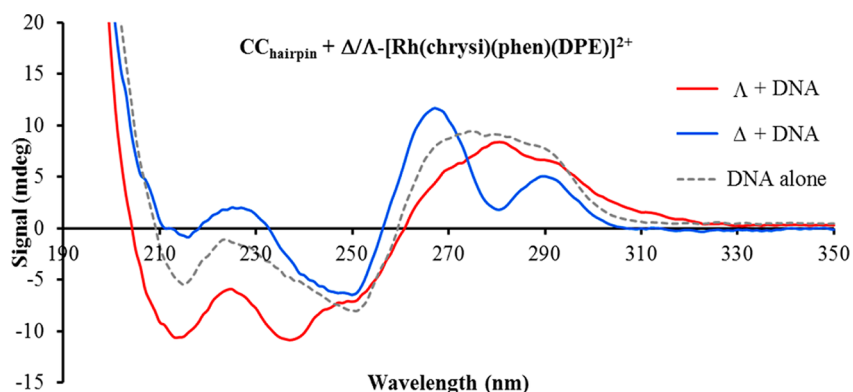

Figure 4. CD spectra of Δ- and Λ-[Rh(chrysi)(phen)(DPE)]²⁺ bound to mismatched DNA. Shown are spectra of 25 μM solutions of Δ- and Λ-[Rh(chrysi)(phen)(DPE)]²⁺ in 100 mM NaCl, 20 mM NaP$_i$, pH 7.1 buffer bound to the DNA hairpin 5′-GGCAGG$\underline{C}$ATGGCTTTTTGC-CATC$\underline{C}$CTGCC-3′ (underline denotes the CC mismatch), and the DNA hairpin alone (Δ in blue, Λ in red, DNA alone in gray).

Due to the drastic differences in mismatched DNA binding characterization between [Rh(chrysi)(phen)(DPE)]²⁺ and [Rh(bpy)₂(chrysi)]³⁺, binding affinities of both enantiomers of the DPE complex at a variety of DNA mismatches were determined. It has been reported that the mismatch-specific DNA binding affinities of Δ-[Rh(bpy)₂(chrysi)]³⁺ correlate with the thermodynamic destabilization of the mismatch.[28] This correlation is due to the unique binding mode of metalloinsertion where the mismatched base pair is completely ejected from the double helix upon metal complex binding.[10] Therefore, four different DNA hairpins of the form 5′-GGCAGT$\underline{X}$CTGGCTTTTTGCCAG$\underline{Y}$ACTGCC-3′ ($\underline{XY}$ = CC, CA, CT, AA) were synthesized, and the binding affinities of Δ- and Λ-[Rh(chrysi)(phen)(DPE)]²⁺ determined as described above. The results, along with mismatch thermodynamic destabilization values,[29] are shown in Table 2; the binding affinities of the Δ enantiomer correlate with the thermodynamic destabilization of the mismatch (1.1 × 10⁶ M⁻¹ for a CC mismatch versus 0.23 × 10⁶ M⁻¹ for an AA mismatch), while those of the Λ enantiomer do not (1.09 × 10⁶ M⁻¹ for a CC mismatch versus 3.54 × 10⁶ M⁻¹ for an AA mismatch). Binding competition gels between both Δ- and Λ-[Rh(chrysi)(phen)(DPE)]²⁺ and 4 μM [Rh(bpy)₂(phi)]³⁺ (a non-sequence specific intercalator that binds at all sites in the duplex) exhibit no binding at matched sites up to 1:15 DNA: [Rh(chrysi)(phen)(DPE)]²⁺ (data not shown), eliminating the possibility of non-mismatch-specific binding by either enantiomer.

In order to ascertain if racemization of the two enantiomers occurs upon DNA binding, CD spectra were taken of the two enantiomers before and after addition to mismatched DNA. As can be seen in Figure 4, the CD spectra of the two metalloinsertor-mismatched DNA complexes are distinct from each other, even after 30 min of incubation (the average time frame of a competition gel titration, wherein both enantiomers bind to DNA). This confirms that the enantiomers bind to mismatched DNA without racemization.

The ability of [Rh(chrysi)(phen)(PPE)]²⁺ to bind covalently to DNA was also assessed by UV−vis spectroscopy. In the event that the Rh−O bond is labile, covalent DNA binding is a possibility. In order to determine if covalent binding occurs, H₂O, [Rh(bpy)₂(chrysi)]³⁺, [Rh(HDPA)₂(chrysi)]³⁺, or [Rh(chrysi)(phen)(PPE)]²⁺ was incubated with mismatched DNA under either neutral conditions (phosphate buffer) or a reducing environment (5 mM gluthathione in phosphate buffer) for 30 min. The DNA was subsequently denatured to release any non-covalently associated rhodium complex and precipitated out of solution. Covalent DNA binding would result in a characteristic rhodium metalloinsertor CT band near 400 nm, which is not present in any of the samples. Furthermore, the absorbance at 260 nm of the various samples confirmed comparable yields of DNA precipitation. Thus, UV−vis spectra of the various samples of precipitated DNA revealed no covalent DNA binding by any of the three complexes (Figure S13) under either neutral or reducing conditions

Inhibition of Cellular Proliferation using an Enzyme-Linked Immunosorbent Assay (ELISA). An ELISA for DNA synthesis was used to quantify the effects of the new family of metalloinsertors on the proliferation of HCT116N cells (MMR-proficient) and HCT116O cells (MMR-deficient) (Figure 5). The compound [Rh(HDPA)₂(chrysi)]³⁺ was included as a control with which to compare the potencies and cell-selectivities of the new compounds. Cisplatin and methylnitronitrosoguanidine (MNNG) were also included as prototypical, FDA-approved chemotherapeutic agents that exhibit decreased effectiveness against MMR-deficient cancer
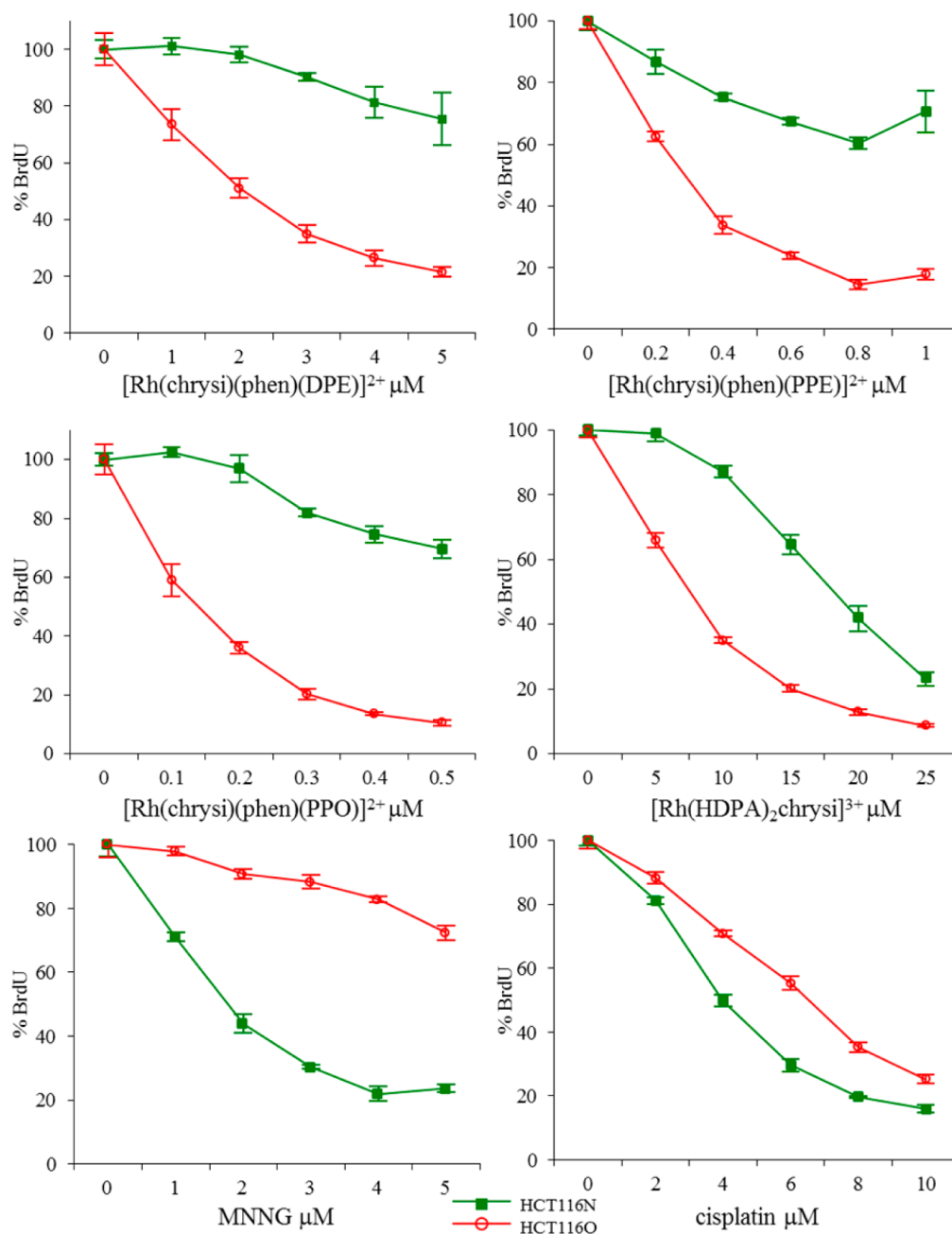
14166

dx.doi.org/10.1021/ja5072064 | J. Am. Chem. Soc. 2014, 136, 14160−14172

Figure 5. Inhibitory effects of *rac*-[Rh(chrysi)(phen)(DPE)]$^{2+}$, *rac*-[Rh(chrysi)(phen)(PPE)]$^{2+}$, *rac*-[Rh(chrysi)(phen)(PPO)]$^{2+}$, *rac*-[Rh-(HDPA)$_2$(chrysi)]$^{3+}$, MNNG, and cisplatin. Shown are plots of BrdU incorporation (a measure of DNA synthesis and therefore cellular proliferation) normalized to the BrdU incorporation of untreated cells as a function of rhodium concentration. Standard error bars for five trials are shown.

cells.[15] Incubations were performed for 24 h, after which time the medium containing the chemotherapeutic was replaced with fresh medium, and the cells were grown for the remainder of the 72 h period. The extent of cellular proliferation is expressed as the ratio of BrdU incorporated by the treated cells as compared to untreated controls. We define differential inhibition as the difference in %BrdU incorporation between the HCT116N and HCT116O cells. The results are shown in Figure 5.

Clearly, the new family of complexes has significantly enhanced potency as compared to the earlier generation metalloinsertor; concentrations required for optimal differential activity are reduced from 10 μM for [Rh(HDPA)$_2$(chrysi)]$^{3+}$

(our previously most potent compound) to 3 μM for [Rh(chrysi)(phen)(DPE)]$^{2+}$, 1 μM for [Rh(chrysi)(phen)-(PPE)]$^{2+}$, and 300 nM for [Rh(chrysi)(phen)(PPO)]$^{2+}$. These compounds are also more potent than the FDA-approved chemotherapeutics in these assay conditions, which require 4 and 6 μM for optimal biological activity of MNNG and cisplatin, respectively.[30] In addition, the enhanced cell-selectivity that was observed previously with [Rh(chrysi)-(phen)(DPE)]$^{2+}$ is conserved across the entire family. At their optimal concentrations, their differential inhibitions are 55 $\pm$ 2%, 53 $\pm$ 7%, and 62 $\pm$ 2% for the DPE, PPE, and PPO derivatives, respectively. Note that any cell selectivity by cisplatin or MNNG favors the MMR-proficient cells. This is
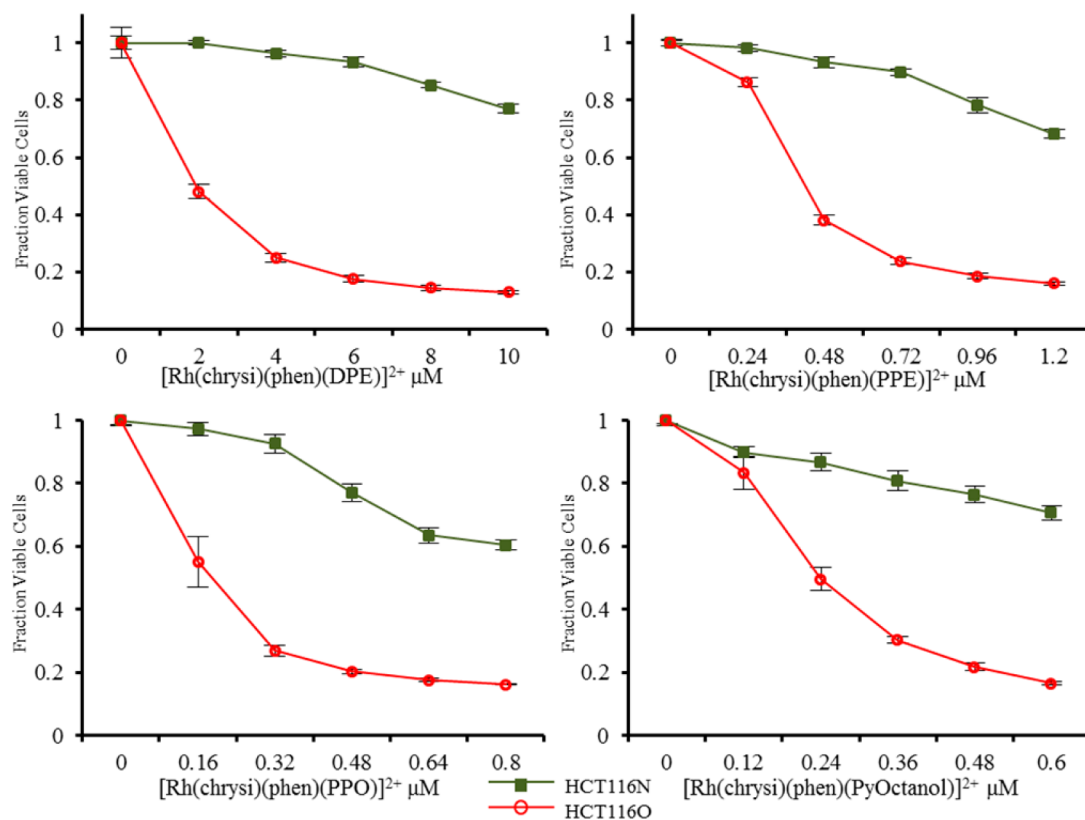
Figure 6. Differential cytotoxicities of *rac*-[Rh(chrysi)(phen)(DPE)]$^{2+}$, *rac*-[Rh(chrysi)(phen)(PPE)]$^{2+}$, *rac*-[Rh(chrysi)(phen)(PPO)]$^{2+}$, and *rac*-[Rh(chrysi)(phen)(PyOctanol)]$^{2+}$. HCT116N (green) and HCT116O (red) cells were plated in 96-well format at densities of 5×10^4 cells/well and treated with the concentrations of rhodium metalloinsertors indicated. After 72 h, the cells were labeled with MTT for 4 h.

characteristic of the DNA-binding therapeutics and leads to significant buildup of drug resistance in the clinic.[31] The family of metalloinsertors instead shows activity preferentially in the MMR-deficient cells. This selectivity is unique to all active metalloinsertors, but this new generation of complexes exhibits levels of selectivity and potency previously unseen.

MTT Cytotoxicity Assay. The cytotoxic effects of all complexes were determined by MTT assay.[24] Briefly, reduction of the MTT reagent by metabolically active cells leads to the production of formazan, which can then be dissolved in acidified SDS to produce a characteristic absorbance at 570 nm. Thus, this absorbance reflects the amount of metabolically active cells in each sample. HCT116N and HCT116O cells were plated and treated with the various rhodium complexes at the concentrations indicated in Figure 6 for 72 h. Percent viability is defined as the ratio of the amount of formazan in the treated cells to that in the untreated cells, and differential cytotoxicity is defined as the difference between the percent viabilities of the two cell lines. The results are shown in Figure 6. All four compounds in this new family display differential cytotoxicity in excess of 50%, and three compounds exhibit maximal activity at nanomolar concentrations. Specifically, the differential cytotoxicities and optimal concentrations of [Rh(chrysi)(phen)(DPE)]$^{2+}$, [Rh(chrysi)(phen)(PPE)]$^{2+}$, [Rh(chrysi)(phen)(PPO)]$^{2+}$, and [Rh(chrysi)(phen)-(PyOctanol)]$^{2+}$ are $76 \pm 2\%$ at 6 μM, $66 \pm 2\%$ at 720 nM, $66 \pm 3\%$ at 320 nM, and $55 \pm 3\%$ at 480 nM, respectively. This is an increase in cytotoxic potency of almost 2 orders of magnitude as compared to [Rh(HDPA)$_2$(chrysi)]$^{3+}$ (25 μM required for optimal cytotoxicity). Moreover, this is the only

instance of a metalloinsertor with a lipophilic ancillary ligand that retains the cell-selective activity unique to our compounds.

The cell-selective cytotoxicities of the two enantiomers of [Rh(chrysi)(phen)(DPE)]$^{2+}$ were also assessed (Figure S14). Just as both enantiomers bind with equal affinity to DNA mismatches, both enantiomers display similar cell-selectivity; their optimal differential cytotoxicities are $78 \pm 1\%$ and $75 \pm 2\%$ for Δ and Λ, respectively, although the Λ enantiomer requires a higher concentration. This is again in direct contrast to [Rh(bpy)$_2$(chrysi)]$^{3+}$, where only the Δ isomer displays differential biological activity.[32]

ICP-MS Assay for Whole-Cell Rhodium Levels. HCT116O and HCT116N cells were treated with each rhodium complex at the concentrations indicated in Figure S15 for 24 h. Whole cell lysates were subsequently analyzed for rhodium levels by ICP-MS and normalized to protein content (Figure S15). These Rh complex concentrations correspond to those necessary for optimal biological activity in the 24 h ELISA experiment for the four different complexes. Therefore, the intracellular rhodium concentrations in this experiment reflect the amount of rhodium in the cell that is required for an optimal biological response. It is striking that the new family of compounds requires significantly less intracellular rhodium to elicit a biological response than the prototypical [Rh(HDPA)$_2$-(chrysi)]$^{3+}$ compound; specifically, the new compounds exhibit comparable biological activity to [Rh(HDPA)$_2$(chrysi)]$^{3+}$ with only $20 \pm 2\%$ ([Rh(chrysi)(phen)(DPE)]$^{2+}$), $15 \pm 5\%$ ([Rh(chrysi)(phen)(PPE)]$^{2+}$), or $13 \pm 2\%$ ([Rh(chrysi)-(phen)(PPO)]$^{2+}$) of the amount of intracellular rhodium.

Mode of Cell Death. The mode of cell death upon rhodium treatment was characterized through a dye-exclusion

14168

dx.doi.org/10.1021/ja5072064 | *J. Am. Chem. Soc.* 2014, 136, 14160−14172

flow cytometry assay.[25] The assay differentiates between live cells, dead cells, and cells undergoing apoptosis or necrosis through concurrent staining with propidium iodide (a dead-cell-permeable dye) and YO-PRO-1 (an apoptotic-cell-permeable dye). By plotting the fluorescence of the YO-PRO-1 channel against the PI channel, a pattern emerges. Healthy cells are seen in the lower lefthand corner of the plot as they incorporate neither dye. Apoptotic cells exhibit higher YO-PRO-1 fluorescence but still exclude propidium iodide, placing them in the upper lefthand quadrant of the pattern. Conversely, necrotic cells admit propidium iodide but not YO-PRO-1 and are thus in the lower righthand quadrant. Dead cells admit both dyes and are therefore seen in the upper righthand quadrant of the image. Upon flow cytometry analysis, cells can be classified as live, apoptotic, necrotic, or dead by defining regions in the fluorescence plane corresponding to each category.

The HCT116N and HCT116O cell lines were incubated with 0−0.5 μM of $[Rh(chrysi)(phen)(PPO)]^{2+}$ for 72 h. After harvesting the cells and staining with both PI and YO-PRO-1, the cells were analyzed by flow cytometry to obtain raw fluorescence data. Representative data for 200 nM rhodium treatment for 72 h are shown in Figure 7. YO-PRO-1 fluorescence is shown on the y-axis, and PI fluorescence is shown on the x-axis. The raw data were analyzed by gating the fluorescence events into one of four categories. Figure 7 also shows histograms of live, apoptotic, necrotic, and dead cells for the HCT116N and HCT116O cell lines based on the flow cytometry. Rhodium treatment was either 0.2 or 0.5 μM $[Rh(chrysi)(phen)(PPO)]^{2+}$ for 72 h. As with $[Rh(HDPA)_2chrysi]^{3+,17}$ $[Rh(chrysi)(phen)(PPO)]^{2+}$ treatment induces necrosis preferentially in the MMR-deficient HCT116O cell line; the number of necrotic cells increases from 1.2 ± 0.1% to 13 ± 2% after treatment with 0.2 μM $[Rh(chrysi)(phen)(PPO)]^{2+}$. There is no significant change in the percentage of cells in the apoptotic region in either cell line following metalloinsertor treatment (26 ± 7% vs 25 ± 7% for the HCT116N cell line, and 10 ± 6% vs 17 ± 7% for the HCT116O cell line). The effect of rhodium treatment is significantly more pronounced in the MMR-deficient HCT116O cell line, in which live cells drop from 82 ± 7% to 28 ± 6% after treatment with 0.2 μM $[Rh(chrysi)(phen)-(PPO)]^{2+}$ versus the MMR-proficient HCT116N cell line, which shows no decrease in live cells (57 ± 9% versus 57 ± 7%) after treatment with 0.2 μM $[Rh(chrysi)(phen)(PPO)]^{2+}$.

■ DISCUSSION

A new family of rhodium complexes containing Rh−O coordination have been prepared, and all show higher potency and selectivity for MMR-deficient cells compared to earlier rhodium metalloinsertors. The DPE ligand was originally designed to coordinate to the Rh center via the two pyridine rings, as per previously synthesized metalloinsertors. The solid-state structure of $[Rh(chrysi)(phen)(DPE)]^{2+}$ revealed the true coordination to include an axial Rh−O bond. The driving force for this ligand coordination may be the formation of a five-membered ring, as opposed to the six-membered ring that would form if the second pyridine ring coordinated.[33] This family of complexes offers new possibilities for binding DNA mismatches and for providing potent targets for cellular processing.

Characterization in Solution and Binding to Mismatched DNA. Spectrophotometric titrations reveal that the acidity of the chrysi immine proton of the new complexes
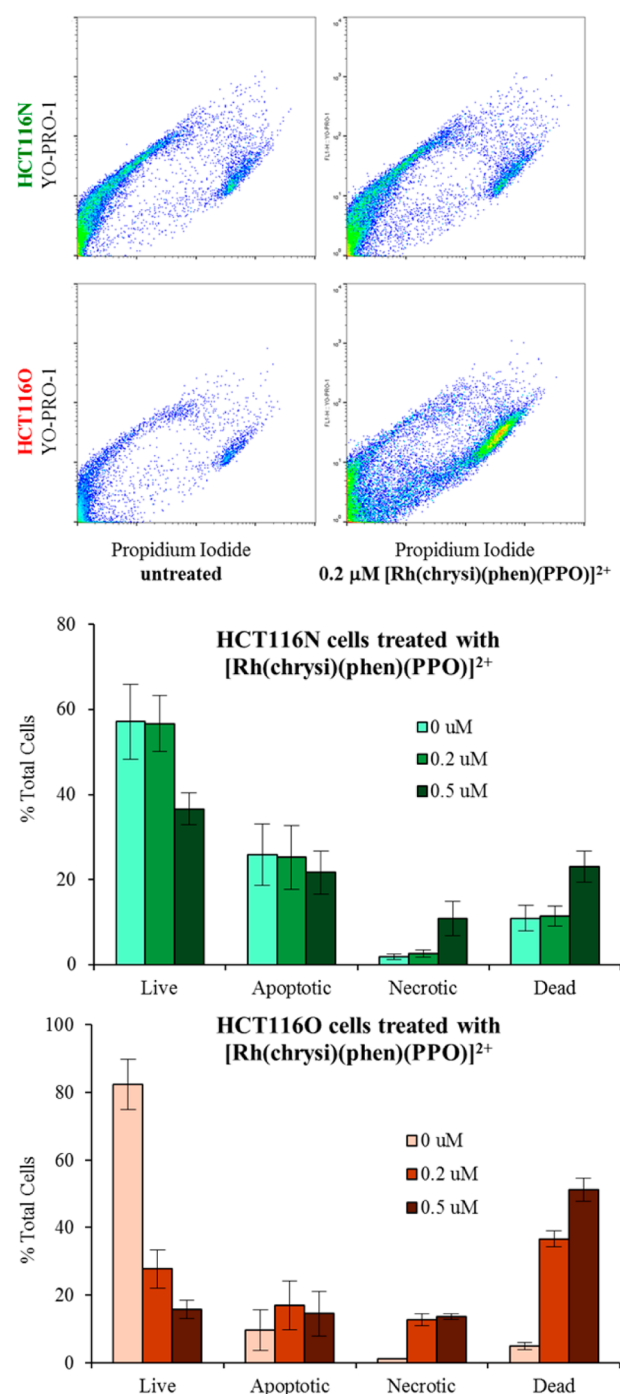

Figure 7. Flow cytometry assay of cell death mechanism. (Top) HCT116N and HCT116O cells were treated with 0.2 μM $[Rh(chrysi)(phen)(PPO)]^{2+}$ for 72 h. The color scale represents the number of cells, with blue indicating fewer cells at a given pair of fluorescence levels, and orange representing a greater number of cells at a given pair of fluorescence levels. Rhodium treatment causes cells to move away from the origin, along the necrotic pathway (lower branch of pattern). The effect is more pronounced in the HCT116O cell line. (Bottom) HCT116N and HCT116O cells were treated with 0.2 or 0.5 μM $[Rh(chrysi)(phen)(PPO)]^{2+}$ for 72 h. Rhodium treatment causes a sharp decrease in the live population of the HCT116O cell line with a corresponding increase in the necrotic and dead cell populations. Less of an effect is seen in the HCT116N cell line. Thus, these data are consistent with $[Rh(chrysi)(phen)(PPO)]^{2+}$ preferentially inducing necrosis in the MMR-deficient HCT116O cell line.

14169

dx.doi.org/10.1021/ja5072064 | J. Am. Chem. Soc. 2014, 136, 14160−14172

(pK_a's of 8.3 to 8.9) vary significantly from that of [Rh(bpy)$_2$(chrysi)]$^{3+}$ (pK_a of 5.2)[27] and [Rh(HDPA)$_2$-(chrysi)]$^{3+}$ (pK_a of 7.0). This difference is most likely due to the negative charge on the DPE ligand; a more basic environment is required to deprotonate the 2+ [Rh(chrysi)-(phen)(DPE)]$^{2+}$ species than the 3+ [Rh(HDPA)$_2$(chrysi)]$^{3+}$ species. Furthermore, in the case of [Rh(bpy)$_2$(chrysi)]$^{3+}$, the chrysi immine proton must be deprotonated in order for the molecule to bind to mismatched DNA.[10,11] When both immine protons are retained, the chrysi ligand is not planar (Figures 2 and 8) due to steric clashing, which, effectively prevents full π-
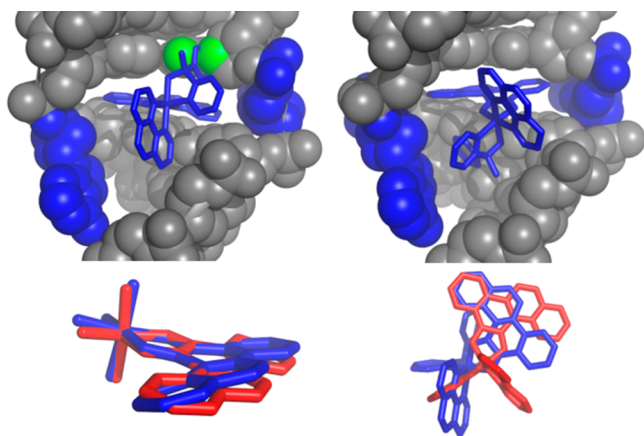

Figure 8. Possible models of Δ-[Rh(chrysi)(phen)(DPE)]$^{2+}$ bound to mismatched DNA. Top left: The crystal structure of Δ-[Rh(chrysi)-(phen)(DPE)]$^{2+}$ has been modeled into the crystal structure of Δ-[Rh(bpy)$_2$(chrysi)]$^{3+}$ bound to an AC mismatch by overlaying the chrysi ligands to maximize π-stacking between the chrysi ligand and the adjacent base pairs. As can be seen in green, there is a great deal of steric clashing between the DPE ancillary ligand and the DNA. Top right: The crystal structure of Δ-[Rh(chrysi)(phen)(DPE)]$^{2+}$ has been modeled into the crystal structure of Δ-[Rh(bpy)$_2$(chrysi)]$^{3+}$ bound to an AC mismatch by rotating the compound to minimize steric clash between the ancillary ligands and the DNA, resulting in a reduced amount of π-stacking between the chrysi ligand and the adjacent base pairs. Bottom right: Superposition of Δ-[Rh(chrysi)(phen)(DPE)]$^{2+}$ (blue) and Δ-[Rh(bpy)$_2$(chrysi)]$^{3+}$ (red) in this model. As can be seen, only two rings of the chrysi ligand of the DPE complex are now situated for π-stacking in the duplex. Bottom left: Superposition of the chrysi ligands of Δ-[Rh(chrysi)(phen)(DPE)]$^{2+}$ (blue) and Δ-[Rh(bpy)$_2$(chrysi)]$^{3+}$ (red). When both immine protons are retained, the chrysi ligand buckles and is no longer planar (blue).

stacking with the base pairs adjacent to the mismatched site upon DNA binding. Despite this fact, the entire family of complexes appears to bind to mismatched DNA without deprotonation (Figures 3 and S12). Additionally, substantial hypochromicity is observed upon DNA binding, confirming that there must be significant π-stacking between the DNA and the chrysi ligand. These observations suggest a different conformation for mismatch binding with this new family of complexes as compared to [Rh(bpy)$_2$(chrysi)]$^{3+}$.

We also explored the possibility of covalent binding through displacement of the Rh−O bond and substitution of a DNA base as a ligand. The ensuing covalent lesion could be a potent target for the machinery of the cell.[6] However, even under an extremely reducing environment (5 mM glutathione), we find no evidence of covalent binding of the complex to DNA.

In order to further characterize the compounds and their interactions with DNA, the enantiomers of [Rh(chrysi)(phen)-

(DPE)]$^{2+}$ were separated by HPLC. In the case of a labile Rh−O bond, racemization of the enantiomers would be expected to occur over time.[34] However, samples of both enantiomers in aqueous solution in light exhibited no racemization over a month, as confirmed by chiral HPLC and CD. Furthermore, the two enantiomers do not racemize upon DNA binding (Figure 4), and, in fact, exhibit distinct CD spectra when bound to DNA, providing direct evidence that both enantiomers are stable and bind individually to mismatches.

Do the complexes bind to mismatched DNA through metalloinsertion? Both the Δ and Λ isomers of [Rh(chrysi)-(phen)(DPE)]$^{2+}$ bind with equally high specificity for mismatched DNA and with similar binding affinities. For Δ-[Rh(chrysi)(phen)(DPE)]$^{2+}$ we also see a correlation between binding affinity and destabilization of the mismatch, and this provides strong support for binding through metalloinsertion for the Δ-isomers. The fact that the DNA mismatch binding affinities of Λ-[Rh(chrysi)(phen)(DPE)]$^{2+}$ do not correlate with the destabilization of the mismatch is surprising. It may be the case that buckling by the chrysi ligand coupled with steric clashes by the Λ-isomer with the helix means that full insertion may not occur, and instead there may be some twisting of the complex within the site. More structural characterization is clearly required here.

Biological Effects of the Complexes in Cells. Most important is the high biological activity of the new generation of complexes coupled with their high selectivity for MMR-deficient cells. As can be seen from Figures 5 and 6, all four complexes exhibit the MMR-deficient cell-selective activity that is unique to rhodium metalloinsertors. Indeed, appending additional steric bulk off the back of the complexes does not interfere with the cellular response to the rhodium-DNA lesion associated with mismatch binding. The fact that [Rh(chrysi)-(phen)(PyOctanol)]$^{2+}$ retains its cell selectivity is also surprising given our recent results that the more lipophilic metalloinsertors localize to the mitochondria, which in effect abolishes their cell selectivity.[18] One possibility is that the ancillary PyOctanol ligand dissociates either prior to or following cellular uptake. Again, our results showing the lack of racemization of the [Rh(chrysi)(phen)(DPE)]$^{2+}$ isomers over a month in a reducing aqueous environment argue against that explanation. Both Δ- and Λ-[Rh(chrysi)(phen)(DPE)]$^{2+}$ display comparable cell-selective activity in the MTT assay. This result implies similar Rh-DNA lesions being formed for the two enantiomers; if the enantiomers were binding to DNA using markedly different binding modes, their biological activities would vary greatly.

We also assessed cellular uptake of the family and compared them to that of [Rh(HDPA)$_2$chrysi]$^{3+}$. The new family of complexes require from 7.5- to 5-fold less intracellular rhodium as compared to [Rh(HDPA)$_2$chrysi]$^{3+}$ to evoke the same cellular response. This may be an indication that the Rh-DNA lesion being formed is more readily recognized by the cellular machinery, and thus fewer lesions are required for cytotoxicity. Furthermore, the three complexes with Rh−O bonds exhibit similar intracellular rhodium concentrations; they vary <1.5-fold from each other. This is despite a 10-fold difference in the rhodium concentration of the media between [Rh(chrysi)-(phen)(DPE)]$^{2+}$ and [Rh(chrysi)(phen)(PPO)]$^{2+}$. This clearly demonstrates that the latter compound has more efficient uptake than the parental DPE compound.

Finally, we evaluated the mode of cell death caused by treatment of HCT116 cells with the new complex [Rh(chrysi)-

(phen)(PPO)]$^{2+}$ as a representative member of the new family. The admission of the dead-cell stain propidium iodide by the HCT116 cell lines upon rhodium treatment reveals that cell death proceeds through a necrotic, rather than apoptotic pathway, similar to [Rh(HDPA)$_2$chrysi]$^{3+}$ treatment (Figure 7).[17] If there is a different Rh-DNA lesion being formed by the new family of complexes, then it is not different enough to evoke a significantly altered global cellular response. Certainly, the enhanced potency and selectivity of these new complexes make them suitable candidates for the next step in chemotherapeutic development.

Models for DNA Insertion by the Complexes. Given the potency of the complexes, it becomes important to explore how they might be oriented on the DNA helix to provide a target for cellular responses. Figure 8 compares two different proposed models of Δ-[Rh(chrysi)(phen)(DPE)]$^{2+}$ bound to a mismatched site in DNA. Preserving the DNA conformation from the crystal structure of [Rh(bpy)$_2$(chrysi)]$^{3+}$ bound to an AC mismatch,[10] in one model, we simply overlaid the chrysi ligand of Δ-[Rh(chrysi)(phen)(DPE)]$^{2+}$ with that of Δ-[Rh(bpy)$_2$-(chrysi)]$^{3+}$ when bound to mismatched DNA. In the other model, Δ-[Rh(chrysi)(phen)(DPE)]$^{2+}$ has been flipped and rotated to alleviate the steric clashing between the two ancillary ligands and the DNA, yet retain π-stacking between two rings of the chrysi ligand and the adjacent base pairs. Figure 8 shows that in the first model, there is the potential for significant steric clashing between the dangling pyridine group of Δ-[Rh-(chrysi)(phen)(DPE)]$^{2+}$ and the DNA backbone (shown in green). This steric clash is partially alleviated when the DPE complex is exchanged for the PPO complex and exacerbated when exchanged for Λ-[Rh(chrysi)(phen)(DPE)]$^{2+}$ (not shown). Given the similarity in binding affinities of the various complexes, it is clear that this cannot be the correct binding conformation for this new family. In the second model, there is no steric clashing between the ancillary ligands and the DNA. This model, in which π-stacking between the chrysi ligand and the base pairs adjacent to the mismatch is reduced in order to circumvent this steric clashing, is consistent with all our results. Due to the presence of both chrysi immine protons upon DNA binding, it is not *possible* for the chrysi ligand to π-stack with the adjacent base pairs using all four rings. This in turn allows for more flexibility in the placement of the metal complex in the minor groove, thus permitting positioning of the complexes in the minor groove without any steric clashing. This reduced stacking may account for the ∼5-fold lower binding affinity of Δ-[Rh(chrysi)(phen)(DPE)]$^{2+}$ for mismatched DNA as compared to Δ-[Rh(bpy)$_2$(chrysi)]$^{3+}$.[35]

It is also important to consider the orientation of the ejected bases in the mismatch-bound complexes. Indeed these bases may be the target for the high cellular response. Significant differences in positioning of the ejected bases are evident when we compare the crystal structures of [Rh(bpy)$_2$(chrysi)]$^{3+}$ and [Ru(bpy)$_2$(dppz)]$^{2+}$ bound to mismatched DNA through metalloinsertion.[36] For the Ru complex, the ejected bases are pulled into the minor groove so as to interact with the ancillary ligands of the metalloinsertor. As illustrated in Figure 8, positioning the complex in a more twisted configuration as a result of the chrysi buckling actually orients the complex closer to the wall of the minor groove; perhaps the ejected bases further stabilize that positioning similar to what is seen for the Ru complex. Understanding these structural aspects will require further structural characterization, however.

CONCLUSIONS

Here we have described a family of rhodium metalloinsertors with a new coordination containing a Rh−O bond axial to the inserting chrysi ligand. This new ligand coordination has been found to lead to enhanced potency and selectivity toward MMR-deficient cancer cells. Indeed, the new complexes appear to be significantly more selective and also more potent than classic chemotherapeutics.[30] The complexes share a higher pK_a of the chrysi ligand, leading to the absence of immine deprotonation and thus the buckling of the inserting ligand within the mismatched site. For many years, the focus of bioinorganic chemists has been on the preparation of more potent analogues of cisplatin that bind covalently to DNA bases.[3,4] However, focus has recently shifted toward the preparation of chemotherapeutics that are more selective than cisplatin owing to design strategies where the complex interacts with a specific biological target found prominently in cancer cells.[7] This new generation of metalloinsertors provides for non-covalent binding to a specific cellular target, DNA mismatches, with high potency and selectively in cells deficient in MMR. This new generation of complexes thus provides an exciting new platform for therapeutic development.

ASSOCIATED CONTENT

Ⓢ Supporting Information

Crystallographic data, representative binding affinity determination, pH titrations, enantiomeric characterization, further DNA binding characterization, and cytotoxicity of the two enantiomers as well as cellular uptake data. This material is available free of charge via the Internet at http://pubs.acs.org.

AUTHOR INFORMATION

Corresponding Author
jkbarton@caltech.edu

Notes

The authors declare no competing financial interest.

ACKNOWLEDGMENTS

REFERENCES

(1) Zhang, C. X.; Lippard, S. J. *Curr. Opin. Chem. Biol.* **2003**, *7*, 481−489.

(2) Mansour, V. H.; Rosenberg, B.; Vancamp, L.; Trosko, J. E. *Nature* **1969**, *222*, 385−386.

(3) Wheate, N. J.; Walker, S.; Craig, G. E.; Oun, R. *Dalton Trans.* **2010**, *39*, 8113−8127.

(4) Kelland, L. R.; Sharp, S. Y.; O'Neill, C. F.; Raynaud, F. I.; Beale, P. J.; Judson, I. R. *J. Inorg. Biochem.* **1999**, *77*, 111−115.

(5) Boulikas, T.; Vougiouka, M. *Oncol. Rep.* **2004**, *11*, 559−595.

(6) Jamieson, E. R.; Lippard, S. J. *Chem. Rev.* **1999**, *99*, 2467−2498.

14171

dx.doi.org/10.1021/ja5072064 | *J. Am. Chem. Soc.* 2014, 136, 14160−14172

(7) Weidmann, A. G.; Komor, A. C.; Barton, J. K. *Comment. Inorg. Chem.* **2014**, *34*, 1−10.

(8) Jackson, B. A.; Barton, J. K. *J. Am. Chem. Soc.* **1997**, *119*, 12986−12987.

(9) Jackson, B. A.; Alekseyev, V. Y.; Barton, J. K. *Biochemistry* **1999**, *38*, 4655−4662.

(10) Pierre, V. C.; Kaiser, J. T.; Barton, J. K. *Proc. Natl. Acad. Sci. U.S.A.* **2007**, *104*, 429−434.

(11) Zeglis, B. M.; Pierre, V. C.; Kaiser, J. T.; Barton, J. K. *Biochemistry* **2009**, *48*, 4247−4253.

(12) Loeb, L. A. *Cancer Res.* **2001**, *61*, 3230−3239.

(13) Bhattacharya, N. P.; Skandalis, A.; Ganesh, A.; Groden, J.; Meuth, M. *Proc. Natl. Acad. Sci. U.S.A.* **1994**, *91*, 6319−6323.

(14) Iyer, R. R.; Pluciennik, A.; Burdett, V.; Modrich, P. L. *Chem. Rev.* **2006**, *106*, 302−323.

(15) Carethers, J. M.; Hawn, M. T.; Chauhan, D. P.; Luce, M. C.; Marra, G.; Koi, M.; Boland, C. R. *J. Clin. Invest.* **1996**, *98*, 199−206.

(16) Hart, J. R.; Glebov, O.; Ernst, R. J.; Kirsch, I. R.; Barton, J. K. *Proc. Natl. Acad. Sci. U.S.A.* **2006**, *103*, 15359−15363.

(17) Ernst, R. J.; Komor, A. C.; Barton, J. K. *Biochemistry* **2011**, *50*, 10919−10928.

(18) Komor, A. C.; Schneider, C. J.; Weidmann, A. G.; Barton, J. K. *J. Am. Chem. Soc.* **2012**, *134*, 19223−19233.

(19) Ernst, R. J.; Song, H.; Barton, J. K. *J. Am. Chem. Soc.* **2009**, *131*, 2359−2366.

(20) Zeglis, B. M.; Barton, J. K. *Nat. Protoc.* **2007**, *2*, 357−371.

(21) Muerner, H.; Jackson, B. A.; Barton, J. K. *Inorg. Chem.* **1998**, *37*, 3007−3012.

(22) Basu, A.; Bhaduri, S.; Sapre, N. Y.; Jones, P. G. *J. Chem. Soc., Chem. Commun.* **1987**, *22*, 1724−1725.

(23) Reitmar, A. H.; Risley, R.; Bristow, R. G.; Wilson, T.; Ganesh, A.; Jang, A.; Peacock, J.; Benchimol, S.; Hill, R. P. *Cancer Res.* **1997**, *57*, 3765−3771.

(24) Mosmann, T. *J. Immunol. Methods* **1983**, *65*, 55−63.

(25) Idziorek, T.; Estaquier, J.; DeBels, F.; Ameisen, J.-C. *J. Immunol. Methods* **1995**, *185*, 249−258.

(26) Smith, P. K.; Krohn, R. I.; Hermanson, G. T.; Mallia, A. K.; Gartner, F. H.; Provenzano, M. D.; Fujimoto, E. K.; Goeke, N. M.; Olson, B. J.; Klenk, D. C. *Anal. Biochem.* **1985**, *150*, 76−85.

(27) Jackson, B. A.; Henling, L. M.; Barton, J. K. *Inorg. Chem.* **1999**, *38*, 6218−6224.

(28) Jackson, B. A.; Barton, J. K. *Biochemistry* **2000**, *39*, 6176−6182.

(29) Peyret, N.; Seneviratne, A.; Allawi, H. T.; SantaLucia, J. *Biochemistry* **1999**, *38*, 3468−3477.

(30) It should be noted that while our concentration ranges for cisplatin and MNNG may differ from those in previous publications (e.g., ref 31 and Aebi, S.; Fink, D.; Gordon, R.; Kim, H. K.; Zheng, H.; Fink, J. L.; Howell, S. B. *Clin. Cancer Res.* **1997**, *3*, 1763−1767), for our assays we test all compounds side-by-side in order for comparisons between these FDA-approved drugs and our metalloinsertors to be drawn.

(31) Fink, D.; Aebi, S.; Howell, S. B. *Clin. Cancer Res.* **1998**, *4*, 1−6.

(32) Junicke, H.; Hart, J. R.; Kisko, J.; Glevob, O.; Kirsch, I. R.; Barton, J. K. *Proc. Natl. Acad. Sci.U.S.A.* **2003**, *100*, 3737−3741.

(33) Hancock, R. D.; Wade, P. W.; Ngwenya, M. P.; deSousa, A. S.; Damu, K. V. *Inorg. Chem.* **1990**, *29*, 1968−1974.

(34) Cimolino, M. C.; Shipley, N. J.; Linck, R. G. *Inorg. Chem.* **1980**, *19*, 3291−3295.

(35) Note that because the chrysi is deprotonated in [Rh(bpy)$_2$(chrysi)]$^{3+}$ once bound to DNA, the overall charge is the same for the two complexes.

(36) Song, H.; Kaiser, J. T.; Barton, J. K. *Nat. Chem.* **2012**, *4*, 615−620.

14172

dx.doi.org/10.1021/ja5072064 | *J. Am. Chem. Soc.* **2014**, *136*, 14160−14172